scientific reports

Check for updates

OPEN

Mapping brain growth and sex differences across prenatal to postnatal development

Yumnah T. Khan[1]✉, Alex Tsompanidis[1], Marcin A. Radecki[1,2], Carrie Allison[1], Meng-Chuan Lai[1,3,4,5,6,7], Richard A. I. Bethlehem[8] & Simon Baron-Cohen[1,8]

The perinatal period, encompassing both prenatal and early postnatal stages, is a highly dynamic and foundational phase of brain development. Despite its significance, limited work has tracked brain growth continuously across prenatal to postnatal development. In this study, we analysed one of the largest perinatal MRI datasets from the Developing Human Connectome Project (798 scans from 699 unique individuals: 263 prenatal and 535 neonatal; 380 males and 319 females) to model age-related changes and sex differences in brain volumes from 21 to 45 weeks postconceptional age. We found that total brain volume grew at an increasing rate up until the early postnatal period, with white matter dominating mid-gestational growth and gray matter dominating late-gestational and postnatal growth. Subcortical gray matter structures showed distinct trajectories and earlier peak growth rates compared to cortical gray matter structures. Additionally, sex differences in brain growth patterns were observed, with males showing greater volumetric increases with age compared with females. The findings demonstrate the evolving structural dynamics of perinatal brain development as well as the importance of integrating prenatal and postnatal neuroimaging to map continuous early brain growth trajectories.

Keywords Brain development, Prenatal, Neonatal, MRI, Brain growth, Sex differences

The perinatal period, spanning both the prenatal and early postnatal stages, is a highly dynamic and foundational phase of brain development. During this critical window, the brain's core architecture is established through developmental processes such as cell proliferation, migration, differentiation, synaptogenesis, dendritic growth, and neuronal circuit formation[1,2]. These processes lay the groundwork for lifelong cognitive, behavioural, and health outcomes[3–6]. Despite its significance, this critical window of brain development remains insufficiently studied due to various challenges associated with applying neuroimaging to fetuses and infants.

While existing studies have separately mapped prenatal and postnatal brain development[7–11], it is also informative to track brain growth continuously from prenatal to postnatal development. This approach captures both the continuous nature of perinatal brain development as well as the brain's response to the prenatal to postnatal transition, enabling the mapping of comprehensive early growth trajectories. While the emergence of large-scale, publicly available datasets has recently enabled investigations into the perinatal development of global brain metrics[12], an understanding of regional development during this formative period remains limited. It is likely that different regions follow distinct developmental timelines that align with their emerging functional roles, structural organisation, and integration into broader neural networks. For instance, it has previously been suggested that regions responsible for basic sensory functions mature first, followed by associative regions responsible for higher-order cognition[13]. Moreover, growth patterns are likely also impacted by the significant environmental changes between the prenatal and postnatal periods. For instance, genetic, placental and maternal factors (e.g., hormones, nutrition, pregnancy trajectories) are key contributors to prenatal brain development[6,14]. In contrast, postnatal development is further shaped by postnatal life experiences (e.g., sensory stimuli, social interactions) which likely promote growth in specific regions[15]. Studying prenatal and postnatal

[1]Department of Psychiatry, Autism Research Centre, University of Cambridge, Cambridge CB2 8AH, UK. [2]Social and Affective Neuroscience Group, IMT School for Advanced Studies Lucca, 55100 Lucca, Italy. [3]Campbell Family Mental Health Research Institute, Centre for Addiction and Mental Health, Toronto, ON, Canada. [4]Department of Psychiatry, The Hospital for Sick Children, Toronto, ON, Canada. [5]Department of Psychiatry, Temerty Faculty of Medicine, University of Toronto, Toronto, ON, Canada. [6]Department of Psychology, Faculty of Arts and Science, University of Toronto, Toronto, ON, Canada. [7]Department of Psychiatry, National Taiwan University Hospital and College of Medicine, Taipei, Taiwan. [8]Department of Psychology, University of Cambridge, Cambridge CB2 3EB, UK. ✉email: yk415@cam.ac.uk

brain development together can therefore provide insights into how the transition between prenatal to postnatal stages impacts growth dynamics in early development.

Importantly, the perinatal period is also a critical window for the emergence of sex differences in the brain. Given that sex differences in brain structure are well-documented across the lifespan[16] and are observed as early as the prenatal and neonatal periods[17,18], sex-differential growth likely begins early in development. A key factor contributing to these differences is the prenatal testosterone surge, during which male fetuses produce approximately 2.5 times more testosterone than female fetuses in the first and second trimesters of pregnancy[19]. This prenatal surge in testosterone, along with sex differences in placental and neuronal gene expression, are understood as key early biological mechanisms initiating sex differences in brain development[20]. There is also growing evidence suggesting that various perinatal exposures - such as pregnancy complications or maternal drug use[21] - impact brain development in sex-specific ways. Given the high plasticity of the perinatal brain, it is likely particularly receptive to these sex-differential biological and environmental factors. Importantly, sex differences are observed in the prevalence and presentation of different neurodevelopmental and psychiatric conditions[22,23]. This may be at least partly attributable to sex differences in early brain development, as variations in brain structure associated with these conditions overlap with sex differences in brain structure[22,24,25]. Given that perinatal brain development is pivotal to shaping lifespan outcomes[6], these early differential growth trajectories might explain why sex differences are observed in health outcomes.

Despite being a critical stage for brain development, there remains a lack of well-powered research on the perinatal period. Existing studies often do not incorporate both prenatal and postnatal scans when modelling early brain growth, obscuring a full picture of early developmental trajectories. The Developing Human Connectome Project (dHCP) dataset[26], which includes both prenatal and neonatal MRI scans, offers a unique opportunity to address this research gap. In the present study, we analysed 798 partially longitudinal prenatal and neonatal MRI scans from 699 unique individuals (263 prenatal, 535 neonatal; 380 males, and 319 females) from 21 to 45 weeks post-conception to model age-related structural changes and sex differences in perinatal brain volumes.

Results

In the present study, we used dHCP prenatal and postnatal scans to map continuous perinatal developmental trajectories of global and regional brain volumes using mixed-effect models. A subset of the sample was partially longitudinal ($N = 97$ out of 699). Within this group, 78 participants had both fetal and neonatal scans, 16 had two fetal scans, one had three fetal scans, and two had two neonatal scans. Two sets of analyses were conducted - one using absolute brain volumes and the one using proportional brain volumes, where the brain volume of interest was expressed as a proportion or fraction of total brain volume. In a pre-analysis step, Bayesian Information Criterion (BIC) values were computed for each global and regional volume (separately for absolute and proportional analyses) to determine whether a linear, quadratic, or cubic model best described its growth trajectory (Supplementary Tables 3 and 4). Mixed-effects models with random intercepts modelled at the subject-level were then fit to each measure using the selected model. The models simultaneously included main effects of age, sex, and sex-by-age interactions. Full model comparison results are reported in Supplementary Materials. Each analysis was FDR-corrected for multiple comparisons using a significance threshold of ≤ 0.05[27]. Standardised beta coefficients were also calculated for each analysis to denote standardised effect sizes, reported fully in the Supplementary Materials.

Absolute global analysis

The growth trajectories of total brain volume (TBV), total white matter volume (WMV), and total gray matter volume (GMV) were best described by quadratic models. Total brain volume (Age: $\beta = 17{,}995$, $SE = 270$, $p_{FDR} < 0.001$, Age^2: $\beta = 179$, $SE = 35$, $p_{FDR} < 0.001$) and total gray matter volume (Age: $\beta = 12{,}641$, $SE = 156$, $p_{FDR} < 0.001$, Age^2: $\beta = 277$, $SE = 20$, $p_{FDR} < 0.001$) both showed increasing growth rates with age, while total white matter volume (Age: $\beta = 5345$, $SE = 125$, $p_{FDR} < 0.001$, Age^2: $\beta = -97$, $SE = 16$, $p_{FDR} < 0.001$) showed decreasing growth rates. All of these volumes showed linear sex-by-age interactions with significantly greater increases in males (TBV: $\beta = 1765$, $SE = 387$, $p_{FDR} < 0.001$, GMV: $\beta = 1216$, $SE = 224$, $p_{FDR} < 0.001$, WMV: $\beta = 556$, $SE = 179$, $p_{FDR} = 0.003$). All quadratic sex-by-age interaction terms were non-significant (TBV: $\beta = 35$, $SE = 50$, $p_{FDR} = 0.54$, GMV: $\beta = 35$, $SE = 50$, $p_{FDR} = 0.54$, WMV: $\beta = -9$, $SE = 23$, $p_{FDR} = 0.71$).

Intracranial volume (ICV) (Age: $\beta = 16891$, $SE = 422$, $p_{FDR} < 0.001$, Age^2: $\beta = 317$, $SE = 96$, $p_{FDR} < 0.001$, Age^3: $\beta = 30$, $SE = 7$, $p_{FDR} < 0.001$) and cerebrospinal fluid (CSF) (Age: $\beta = -1078$, $SE = 175$, $p_{FDR} < 0.001$, Age^2: $\beta = 142$, $SE = 37$, $p_{FDR} < 0.001$, Age^3: $\beta = 30$, $SE = 3$, $p_{FDR} < 0.001$) both showed cubic trajectories. CSF volumes declined at 30–40 weeks and then continued increasing at an accelerating rate from 40 weeks onwards. ICV showed a significant linear sex-by-age interaction with greater increases in males ($\beta = 1621$, $SE = 599$, $p_{FDR} = 0.01$), but non-significant quadratic ($\beta = 243$, $SE = 134$, $p_{FDR} = 0.11$) and cubic ($\beta = 15$, $SE = 10$, $p_{FDR} = 0.18$) interaction terms. CSF showed significant quadratic ($\beta = 142$, $SE = 37$, $p_{FDR} < 0.001$) and cubic ($\beta = 30$, $SE = 3$, $p_{FDR} < 0.001$) sex-by-age interactions, indicating a more pronounced cubic trajectory in males (see Fig. 1).

Proportional global analysis

In order to understand changes in the relative contributions of gray and white matter to overall brain growth while avoiding model collinearity, total gray and white matter volumes were analysed as proportions of total brain volume (Fig. 2). Cubic models best fit these proportional trajectories. Across the studied period, total gray matter proportions increased (Age: $\beta = 0.01$, $SE = 0.00$, $pFDR < 0.001$, Age2: $\beta = -0.00$, $SE = 0.00$, $pFDR = 0.02$, Age3: $\beta = -0.00$, $SE = 0.00$, $pFDR < 0.001$) while total white matter proportions decreased (Age: $\beta = -0.01$, $SE = 0.00$, $pFDR < 0.001$, Age2: $\beta = 0.00$, $SE = 0.00$, $pFDR = 0.02$, Age3: $\beta = 0.00$, $SE = 0.00$, $pFDR < 0.001$). White matter showed greater contributions (>50%) to total brain volume before 35 weeks, while gray matter showed

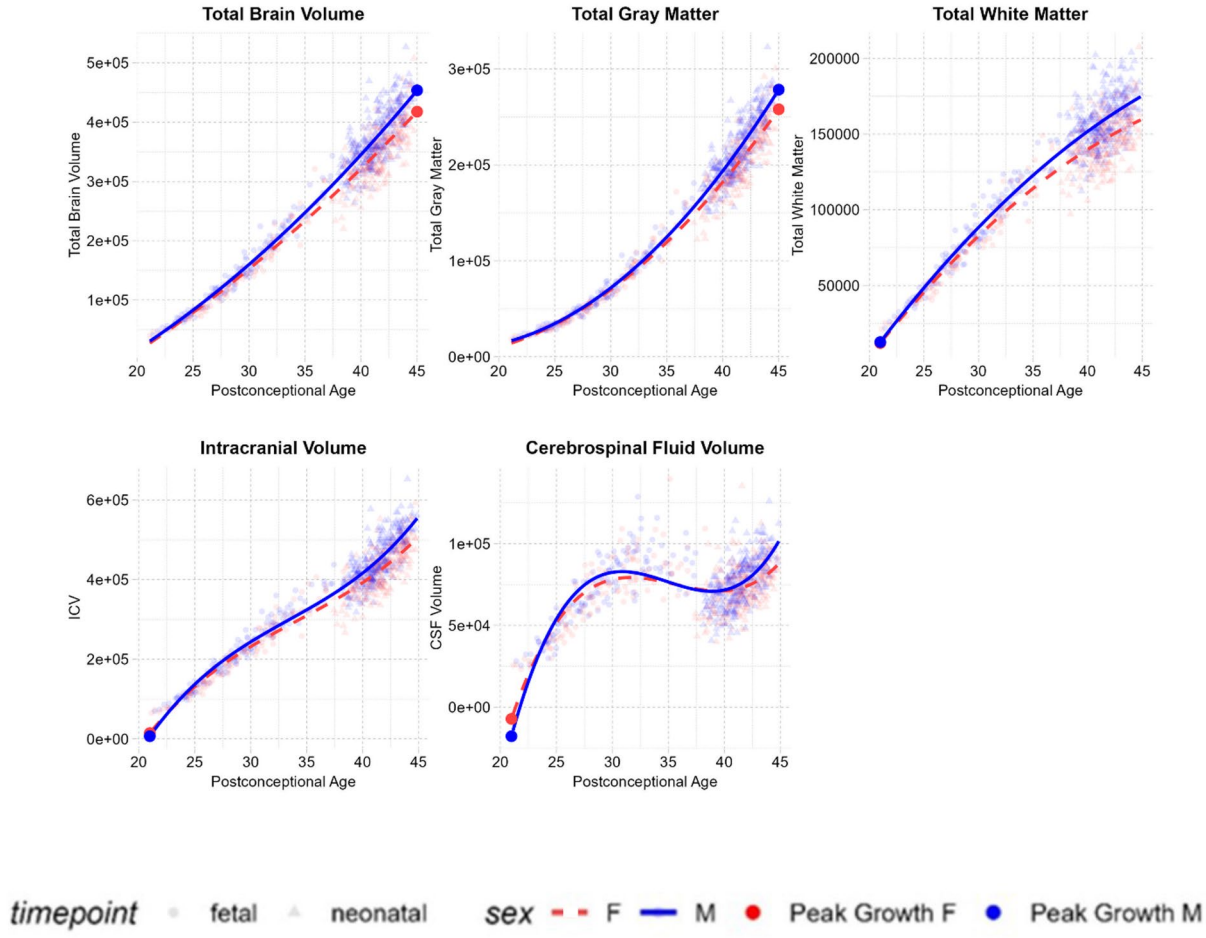

Fig. 1. Global growth trajectories. Global brain volumes (in mm^3) plotted against postconceptional age (in weeks) from 21–45 weeks post-conception. Volumes are plotted according to the trajectory (linear, quadratic, or cubic) determined to be the best fit by model comparisons.

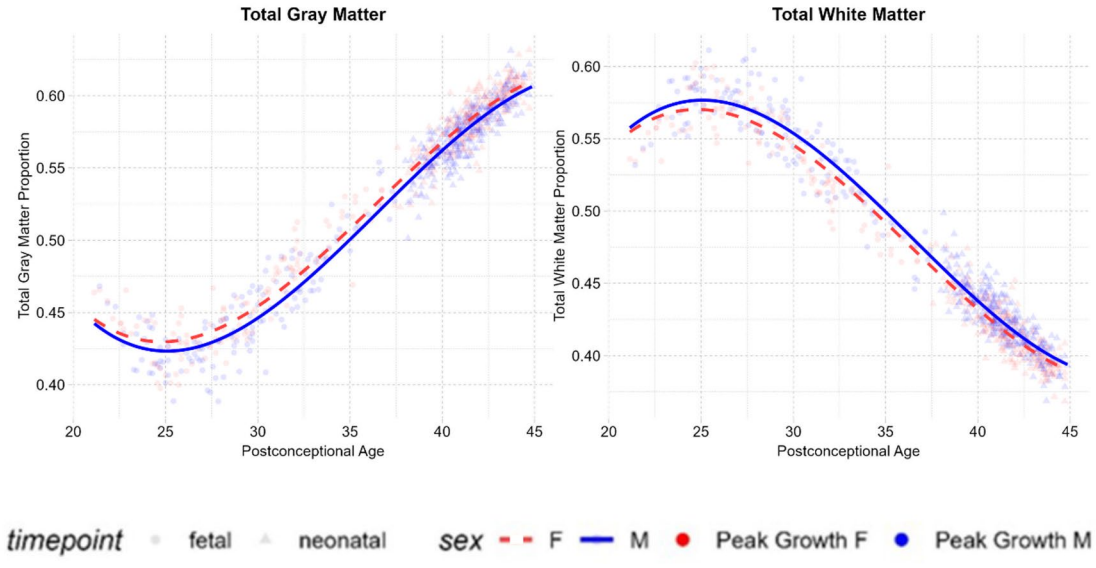

Fig. 2. Proportional gray and white matter trajectories. Total gray and white matter proportions (relative to total brain volume) plotted against postconceptional age (in weeks) from 21–45 weeks post-conception. Volumes are plotted as cubic trajectories, which were determined to be the best fit by model comparisons.

greater contributions after 35 weeks. All sex-by-age interactions were nonsignificant for both gray (Sex × Age: β = 0.00, *SE* = 0.00, *pFDR*=0.23, Sex × Age2: β = − 0.00, *SE* = 0.00, *pFDR* = 0.95, Sex × Age3: β = − 0.00, *SE* = 0.00, *pFDR*=0.65) and white matter proportions (Sex × Age: β = − 0.00, *SE* = 0.00, *pFDR* = 0.24, Sex × Age2: β = 0.00, *SE* = 0.00, *pFDR* = 0.95, Sex × Age3: β = 0.00, *SE* = 0.00, *pFDR* = 0.65).

Absolute regional analysis

All regional analyses reported here are on absolute brain volumes. Regional trajectories as a proportion of total brain volume are reported in Supplementary Materials (Supplementary Table 2). Following the global trends reported above, gray matter in the four cortical lobes showed quadratic trajectories with increasing growth rates, while white matter showed quadratic trajectories with decreasing growth rates (Table 1). Results and figures from the full parcellation (87 structures) are reported in Supplementary Materials (Supplementary Table 1). Various subcortical regions, such as the amygdala, thalamus, and basal ganglia structures, showed cubic growth trajectories. These trajectories were characterised by an initial phase of accelerating growth which peaked during the third trimester, followed by a subsequent phase of decelerating growth postnatally. The corpus callosum and cerebellum showed quadratic trajectories with increasing growth rates, while the hippocampus showed linear growth throughout the studied period (Table 1; Fig. 3).

Absolute regional sex differences

All sex differences reported here are on absolute brain volumes. Sex differences on regional trajectories as a proportion of total brain volume are reported in Supplementary Materials (Supplementary Table 2). Most regions showed linear sex-by-age interactions with significantly faster growth in males (Table 1). Significant quadratic sex-by-age interactions (Fig. 4; Table 2) were identified in the anterior parts of the right medial and

	Age β (SE)	Age^2β (SE)	Age^3β (SE)	Sex × age β (SE)
Occipital R GM	736.1 (12.8)***	15.7 (1.7)***	–	78.6 (18.4)***
Occipital L GM	772.2 (12.2)***	18.8 (1.6)***	–	58.4 (17.6)**
Frontal R GM	1536.8 (23.3)***	31.6 (3.0)***	–	189.9 (33.4)***
Frontal L GM	1544 (23.2)***	32.9 (3.0)***	–	174.6 (33.2)***
Parietal R GM	1181.5 (16.0)***	29.0 (2.0)***	–	103.9 (22.8)***
Parietal L GM	1188.2 (16.1)***	29.3 (2.1)***	–	121.7 (23.2)***
Temporal R GM	1038.9 (14.0)***	27.0 (1.8)***	–	97.0 (20.4)***
Temporal L GM	730 (10.8)***	16.2 (1.4)***	–	72.4 (15.5)***
Occipital R WM	238.2 (9.4)***	− 6.9 (1.2)***	–	43.6 (13.3)**
Occipital L WM	288.8 (8.7)***	− 3.1 (1.1)**	–	32.7 (13.3)*
Frontal R WM	997.2 (27.1)***	− 23.1 (3.5)***	–	106.6 (37.9)**
Frontal L WM	1011.1 (27.2)***	− 23.3 (3.5)***	–	110.8 (38.1)**
Parietal R WM	1181.5 (16.0)***	29.0 (2.0)***	–	103.9 (22.8)***
Parietal L WM	1188.3 (16.1)***	29.3 (2.1)***	–	121.7 (23.2)***
Temporal R WM	555.5 (12.1)***	− 5.9 (1.5)***	–	58.1 (18.1)**
Temporal L WM	525.1 (12.3)***	− 7.3 (1.6)***	–	42.7 (17.7)*
Left Amygdala	36.0 (0.9)***	− 0.5 (0.2)**	− 0.0 (0.0)***	2.3 (1.2)
Right Amygdala	29.4 (0.9)***	− 0.3 (0.2)	− 0.0 (0.0)*	2.9 (1.3)
Thalamus R	247.0 (3.6)***	− 1.9 (0.8)*	− 0.5 (0.1)***	18.7 (5.1)**
Thalamus L	241.0 (3.6)***	− 1.6 (0.8)	− 0.5 (0.1)***	15.8 (5.1)**
Caudate Nucleus R	112.8 (2.4)***	− 0.6 (0.6)	− 0.2 (0.0)***	4.6 (3.4)
Caudate Nucleus L	110.2 (2.4)***	− 0.3 (0.6)	− 0.2 (0.0)***	3.7 (3.3)
Lentiform Nucleus R	155.7 (3.2)***	2.4 (0.4)***	–	15.9 (4.5)**
Lentiform Nucleus L	165.2 (3.5)***	0.5 (0.8)	− 0.1 (0.1)	19.9 (5.0)***
Subthalamic Nucleus R	2.1 (0.4)***	0.2 (0.1)*	0.1 (0.0)***	2.1 (0.4)***
Subthalamic Nucleus L	− 0.4 (0.4)	0.1 (0.1)	0.1 (0.0)***	1.0 (0.5)
Hippocampus R	36.1 (0.6)***	–	–	5.3 (0.9)***
Hippocampus L	32.1 (0.6)***	–	–	4.3 (0.9)***
Cerebellum R	843.4 (11.3)***	21.0 (1.4)***	–	62.2 (15.9)***
Cerebellum L	896.9 (11.4)***	24.2 (1.5)***	–	53.4 (16.1)**
Corpus Callosum	165.7 (3.9)***	4.6 (0.5)***	–	13.8 (5.4)*

Table 1. Regional models. Mixed-effect model outputs, showing beta coefficients (β), standard errors (SE), and significance levels (*p_{FDR}<0.05, **p_{FDR} <0.01, ***p_{FDR} <0.001) of the linear, quadratic, and cubic age terms and linear sex-by-age interactions. In sex-by-age interactions, positive interaction coefficients indicate faster growth in males. All p values are FDR-corrected across the full regional parcellation (87 regions, see Supplementary Materials). R, right hemisphere; L, left hemisphere; GM, Gray matter; WM, White matter.

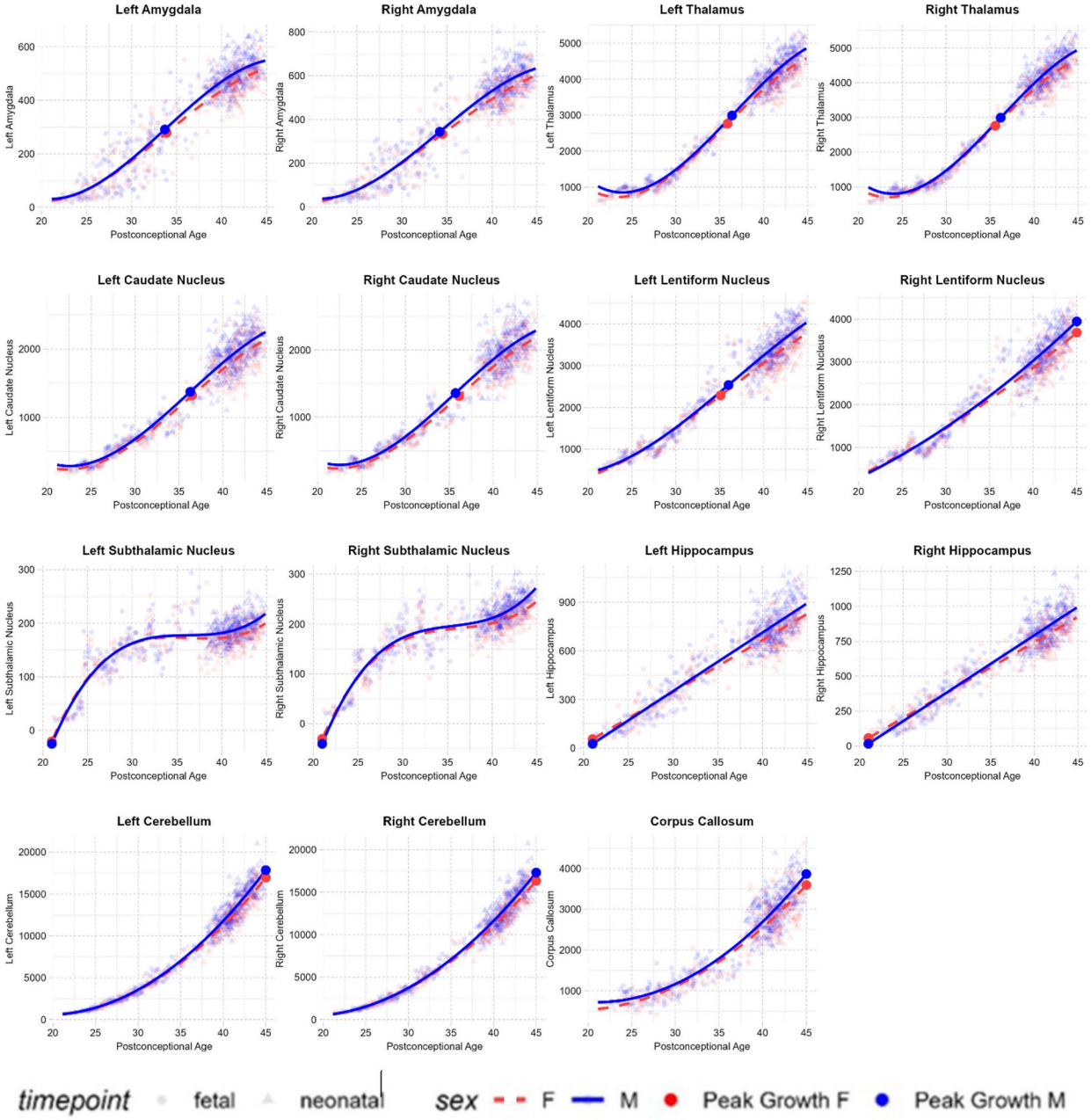

Fig. 3. Subcortical Growth Trajectories. Subcortical brain volumes (in mm^3) plotted against postconceptional age (in weeks) from 21–45 weeks post-conception. Volumes are plotted according to the trajectory (linear, quadratic, or cubic) determined to be the best fit by BIC.

inferior temporal gyri, left parietal lobes, and posterior parts of the bilateral superior temporal gyri, where males showed more rapid and pronounced gray matter increases compared to females. A significant cubic sex-by-age interaction (Table 2) was identified in the left anterior cingulate gyrus, where the plots show a cubic trajectory in males and a linear trajectory in females.

Regional trajectories as a proportion of total brain volume are reported fully in Supplementary Materials (Supplementary Table 2). In summary, these trajectories followed the global trends reported above, with gray matter regional proportions increasing over time and white matter regional proportions decreasing over time. Various significant sex-by-age interactions were also evident, though in fewer regions compared to the absolute regional analysis.

Sensitivity analysis

While the analyses above focused on postconceptional age (the interval between conception and scan), we conducted additional analyses to account for postnatal age at scan (the interval between birth and scan) for the neonatal scans. To do this, we extracted fitted values from models that regressed the brain volumes of interest

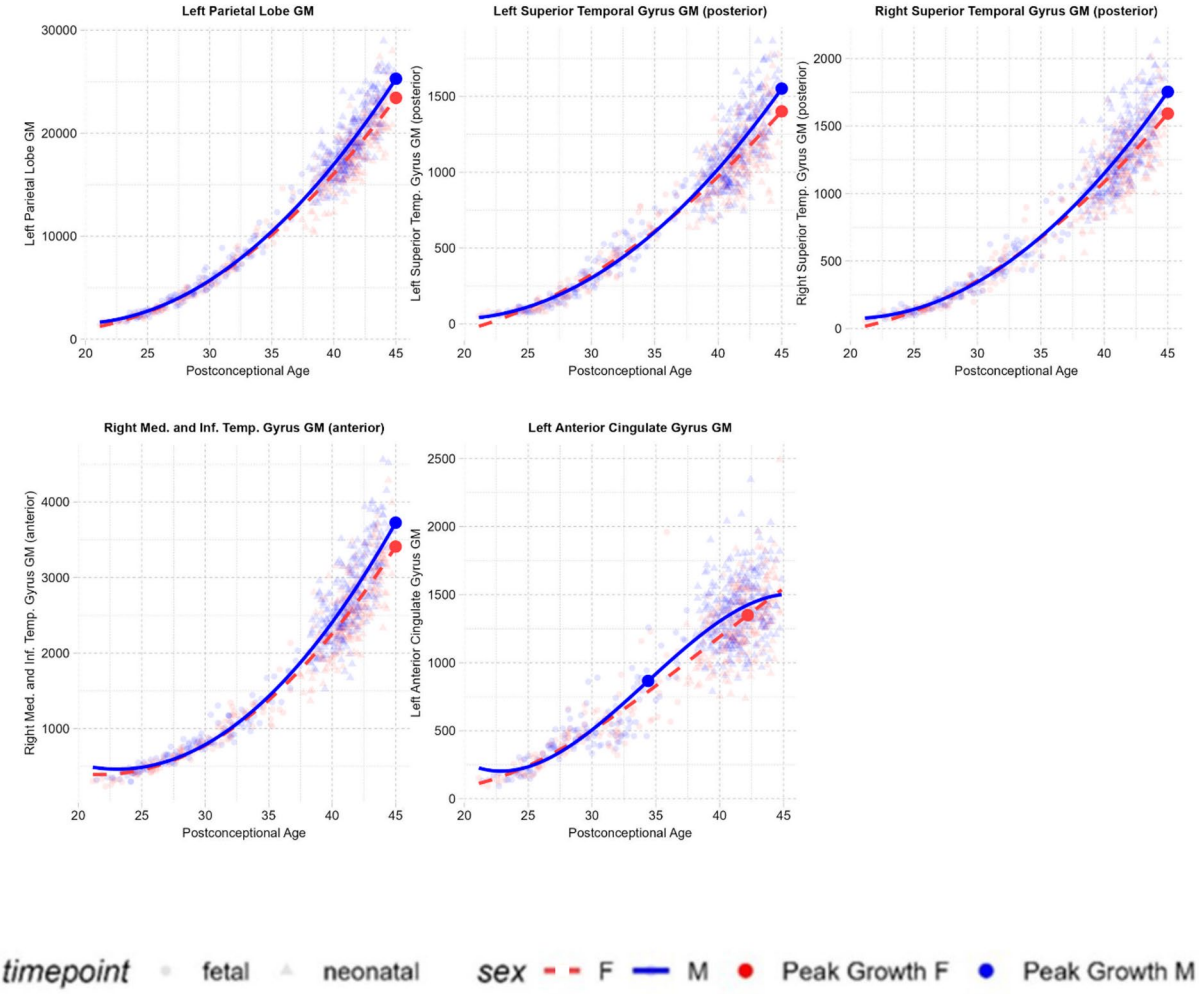

Fig. 4. Regions showing significant quadratic and cubic sex-by-age interactions. Brain volumes (in mm^3) that show significant quadratic or cubic sex-by-age interactions plotted against postconceptional age (in weeks) from 21–45 weeks post-conception. Volumes are plotted according to the trajectory (linear, quadratic, or cubic) determined to be the best fit by model comparisons.

	Sex × age β (SE)	Sex × age^{2}β (SE)	Sex × age^{3}β (SE)
Medial and inferior temporal gyri R GM (anterior parts)	21.3 (4.7)***	1.3 (0.6)*	–
Parietal Lobe L GM	121.9 (23.2)***	6.6 (3.0)*	–
Superior Temporal Gyrus R GM (posterior parts)	11.4 (2.4)***	0.8 (0.3)*	–
Superior Temporal Gyrus L GM (posterior parts)	10.8 (2.3)***	0.8 (0.3)*	–
Anterior Cingulate Gyrus L GM	6.4 (3.9)	– 2.1 (0.83)*	– 0.1 (0.0)*

Table 2. Regions showing significant quadratic and cubic sex-by-age interactions. Mixed-effect model outputs, showing beta coefficients (β), standard errors (SE), and significance levels ($^*p_{FDR}<0.05$, $^{**}p_{FDR}<0.01$, $^{***}p_{FDR}<0.001$) of the linear, quadratic, and cubic (where applicable) sex-by-age interaction terms. Positive interaction coefficients indicate faster growth in males. All p values are FDR-corrected across the full regional parcellation (87 regions, see Supplementary Materials). R, right hemisphere; L, left hemisphere; GM, Gray matter; WM, White matter.

on postnatal age at scan. These analyses captured a deceleration of growth towards the end of the studied period (Fig. 5). This trend was generally observed across all brain volumes (Supplementary Materials Figs. 1 and 2), though subcortical structures continued to show more pronounced cubic trajectories. Further visualisations (Supplementary Materials Fig. 3) indicated that this trend reflected a deceleration in brain growth after the first few postnatal weeks.

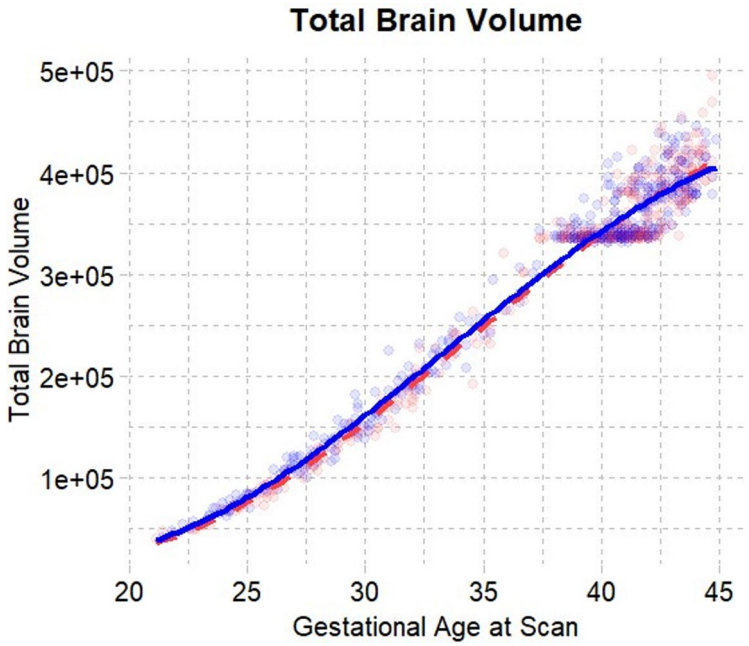

Fig. 5. Growth trajectory of total brain volume after accounting for postnatal age at scan. Figure plots total brain volume in mm^3 (fitted values regressed for postnatal age at scan for neonatal scans) against postconceptional age in weeks from 21–45 weeks post-conception.

We also performed additional model comparisons including logarithmic and exponential models to verify whether the previously selected models provided the best fit to the data. In the majority of cases, neither exponential or logarithmic models improved model fit relative to the linear, quadratic, or cubic models identified in the primary analysis (Supplementary Materials Table 5). In the case of white matter, a logarithmic model yielded a slightly lower BIC value than a quadratic model. However, visualisation showed that both quadratic and logarithmic curves were identical, and the overall conclusions therefore remain unchanged (Supplementary Materials Fig. 4).

Discussion

The prenatal and early postnatal stages are among the most critical periods for brain development, yet these stages have seldom been studied continuously and in well-powered samples. In the present study, we modelled brain growth trajectories during the prenatal to postnatal transition. Using one of the largest prenatal and neonatal MRI datasets (798 scans), we identified various global and regional changes in volumetric dynamics between 21 and 45 weeks postconceptional age. The identified trajectories show that white matter dominates mid-gestational brain growth, while gray matter dominates late gestational and postnatal brain growth. Within gray matter growth, subcortical structures follow distinct trajectories and reach peak growth rates earlier than cortical structures. Additionally, the studied period captured a critical window for sex differences in brain growth, with males showing greater overall volumetric increases with age than females.

The findings demonstrate that while total brain volume initially appeared to show increases at an accelerating rate between 21 and 45 weeks postconceptional age, accounting for postnatal age at scan captures a phase of deaccelerating growth towards the end of the studied period. A similar pattern is reported in prior prenatal studies, where brain growth is shown to rapidly increase between the late second trimester and term[9]. Postnatally, the rate of total brain growth is most rapid in the days immediately after birth and then slows down during subsequent weeks[7]. The second half of gestation and first few postnatal weeks are therefore particularly rapid windows for brain development, likely driven by processes such as dendritic and synaptic development, axonal outgrowth, and glial proliferation[1]. On the other hand, ICV and CSF both showed cubic trajectories. CSF levels were reduced when measured between 30 and 40 weeks and then increased at an accelerating rate from 40 weeks onwards. A transient drop in CSF volumes around birth has also been documented in prior studies[12] and may be linked to the process of labour[28]. Given that the measure of ICV used here represented the sum of total brain volume and CSF, the observed cubic trajectory of ICV is likely also attributable to changes in CSF.

The findings also show that total gray matter generally grows at an increasing rate (with a slight deceleration near the end of the studied period) while white matter grows at a decreasing rate. Notably, the relative contribution of these tissue classes to total brain volume changes across perinatal development. White matter is a greater contributor to total brain volume before ~ 35 weeks, and proportional white matter overall declines across the studied period. Consistent with these findings, prior prenatal studies have shown that white matter is the greatest contributor to total brain growth during the second half of pregnancy, peaking between 29 and 30 weeks[9]. Moreover, diffusion imaging studies show that all major white matter tracts are present at birth, with certain tracts (e.g., thalamo-cortical fibres) already developed by the end of the second trimester[2,29,30]. White matter

injury is also one of the most prominent brain-based differences between term-born and preterm infants[31], reflecting the importance of prenatal white matter development. The subsequent decline in white matter growth rates has also been documented in prior research, where it is shown that white matter increases by only ~ 11% from birth to 1 year, while gray matter increases by 108–149%[3,32]. Similarly, while gray matter volume reaches its peak in childhood, white matter volume only peaks in adulthood[33]. Rapid prenatal increases in white matter therefore likely establish core white matter connectivity, after which the myelination and maturation of these existing connections continue in a more gradual and protracted manner.

Proportional decreases in white matter coincide with proportional increases in gray matter. Gray matter is a greater contributor to total brain volume after ~ 35 weeks, and proportional gray matter volumes overall increases across the studied age-period. These increases are likely due to rapid neural proliferation, dendritic spine arborization, neuropil maturation, and synaptogenesis[2]. These findings are also consistent with prior studies showing that gray matter volume increases more rapidly compared with white matter in the third trimester[9] and postnatally[3,32,34]. Rapid gray matter growth during these periods may hold functional significance, likely enabling the development of key motor, sensory, and cognitive abilities to facilitate postnatal functioning.

Following the global trends reported above, most cortical regions showed quadratic growth trajectories characterised by accelerating regional gray matter growth and decelerating regional white matter growth. Importantly, key differences were identified between regional cortical and subcortical gray matter development. While most cortical regions showed quadratic trajectories, subcortical regions such as the amygdala, thalamus, and basal ganglia structures showed cubic trajectories. These trajectories were characterised by an initial phase of accelerating growth during the third trimester, followed by a subsequent phase of decelerating growth postnatally. Moreover, these structures showed earlier peak growth rates compared with cortical gray matter structures. This may be driven by earlier and faster neurogenesis, dendritogenesis, and synaptogenesis in subcortical structures, followed by a natural slowing of growth as these processes taper. The relatively increased growth of these structures during the third trimester indicates that the prenatal environment plays a critical role in driving subcortical development, which, in turn, may be critical to orchestrating fundamental postnatal functioning. The importance of third trimester subcortical development is further emphasised by findings demonstrating that infants born very pre-term show reduced subcortical volumes at term-equivalent age, particularly in structures such as the thalamus and basal ganglia[35,36]. In turn, these reduced volumes have been associated with poorer cognitive, behavioural, and motor outcomes[36].

Subcortical structures also include the cerebellum, which showed exponential growth throughout the studied age-period. The cerebellum contains more than half of the brain's neurons at birth and is the region that shows the most rapid growth during the second half of gestation and early postnatal life[7,9]. Rapid perinatal cerebellar growth is likely integral to facilitating early motor coordination. Additionally, studies have shown that reduced early cerebellar volumes are associated with cognitive, motor, and socio-affective disruptions[37], highlighting the cerebellum's broader contribution to early functional development.

The hippocampus, on the other hand, was one of the few subcortical structures that showed a linear growth trajectory. Prior research has shown that the hippocampus is the slowest structure to mature during early postnatal development[7]. This is thought to reflect a more gradual development of processes such as memory formation and spatial navigation, which may be comparatively less critical for perinatal functioning (though remains crucial across longer-term development). Overall, these patterns suggest that perinatal regional growth mirrors early developmental patterns, with regions contributing to basic perinatal functioning (e.g., sensorimotor integration) showing earlier peak growth rates compared with regions contributing to higher-order cognition.

On average, males showed significantly faster prenatal and postnatal brain growth than females across the studied period. This pattern was reflected in all global brain volumes as well as several regional volumes. These findings are well-aligned with a large body of research that has shown that males have significantly larger brain volumes than females[16], even as early as during the neonatal period[17]. Larger gray and white matter volumes in males have been associated with higher testosterone levels[38,39]. Similarly, research using an organoid model of the developing human brain has demonstrated that androgens induce cortical expansion[40]. The prenatal surge in testosterone in male fetuses peaks at around 14–18 weeks gestation and is followed by the first observable MRI-based sex differences in brain volumes at around 18 weeks gestation[41]. Observable sex differences in brain structure therefore appear a few weeks after these hormonal changes, likely due to the time required for intermediate cellular and molecular mechanisms to manifest into structural changes in brain volumes. Similarly, prior research has also measured prenatal anogenital distance (AGD), a proxy measure of androgen exposure, which is typically larger in males compared to females. Such research has demonstrated that sex differences in AGD begin prenatally and lag a few weeks behind the prenatal testosterone surge[42].

Between 18 and 40 weeks gestation, the difference in testosterone levels in male and female fetuses remains consistent. Interestingly, a prior study which isolated the neonatal sample used in this research reported several main effects of sex on brain volumes at birth, but few sex-by-age interactions during the first month of postnatal life[17]. Since observable changes in brain volumes occur after hormonal changes, the limited sex-by-age interactions observed during the neonatal period may reflect the stabilisation of prenatal testosterone differences between males and females after mid-gestation. On the other hand, the inclusion of prenatal scans in the present study revealed several significant sex-by-age interactions, highlighting the prenatal period as a critical window for sex-differential growth.

Indeed, while sex differences in brain volumes are reported across the lifespan, sex-by-age interactions are most prominent only during a select few stages, particularly during puberty[43,44] and prenatal development[18]. This is consistent with accounts suggesting that a few critical periods, often coinciding with sex steroid level changes, drive differential growth and produce sex differences that are subsequently observed throughout development[44,45]. Although males exhibit faster overall brain growth (captured by significant linear interactions), the shapes of the growth trajectories (captured by quadratic and cubic interactions) are largely similar between

the sexes. In other words, both sexes generally follow similar global and regional trajectories as reported above, with the exception of a few regions. For instance, males exhibited more rapid and pronounced gray matter increases in the posterior parts of the bilateral superior temporal gyri and anterior parts of the medial and inferior temporal gyrus - regions which also show increased volumes in males at birth[17]. In the left anterior cingulate gyrus, males showed a cubic S-shaped trajectory with decelerating growth towards the end of the studied age-period, while females showed a linear trajectory with steady increases throughout. The region is consistently observed to be relatively larger in females across development[17,46] and is typically associated with social cognition[47,48], a domain in which females show advantages from early life[49]. It is important to note, however, that fewer sex-by-age interactions emerged when analysing regional volumes as a proportion of total brain volume, indicating that sex differences in absolute regional growth may be largely driven by the global sex difference in total brain volume.

It is possible that the growth patterns identified here shape sex-differential neurobiological development from early life, contributing to the emergence of sex differences in neurodevelopmental and psychiatric conditions later in life. While the exact mechanisms and causal pathways underlying this putative relationship remain insufficiently understood, sex hormones are thought play pivotal roles. For instance, fetal testosterone has been implicated in early-emerging conditions such as autism[24], while the identification of several later-emerging conditions that show sex differences (e.g., depression, anxiety, eating disorders) also align with periods of significant hormonal changes, such as puberty[50]. This suggests that sex hormones are important modulators in the interplay between sex differences, brain development, and individual developmental outcomes. Analysing the developmental patterns of sex differences in the brain alongside the developmental patterns of neurodevelopmental and psychiatric conditions may help to explain the exact mechanisms driving these associations.

There are important considerations that need to be taken into account when interpreting the findings of this study. First, the prenatal scans in the dataset begin after 21 weeks, limiting our understanding of brain growth during the first half of the prenatal period. Similarly, there were few prenatal scans after 37 weeks, limiting our understanding of brain growth in the final weeks of gestation in pregnancies lasting over 37 weeks. It is possible that brain development in utero after 37 weeks follows a somewhat different pattern to brain development ex utero, which may warrant further research. Second, it is important to note that there were comparatively fewer scans at the younger age ranges, which may impact the reliable estimation of growth trajectories. Nonetheless, the Restricted Maximum Likelihood method used in mixed effects models is generally well-suited to handling such imbalances[51], and the overall patterns observed in our data remain largely consistent with prior studies that had more balanced sample distributions[10,18]. Second, although the dataset includes some longitudinal measurements, the longitudinal sample comprises only a subset of the full sample (~ 14%). Further research on larger longitudinal samples will be important for validating the developmental trajectories identified here. Third, although both the prenatal and neonatal scans shared the same scanner and largely similar pre-processing procedures, their acquisition parameters differed. For instance, the slice thickness was different for fetal and neonatal acquisitions, and such discrepancies may impact volumetric measurements - particularly in smaller structures[52]. Commonly used harmonisation techniques (e.g., ComBat harmonisation) were deemed unsuitable in this case as they would likely not have been able to distinguish technical differences from true biological differences between prenatal and neonatal development. Nonetheless, we observed continuity across most of our growth curves, and the observed growth trajectories were consistent with those reported in prior prenatal and neonatal research, indicating that technical differences did not play a substantial role in the observed findings. Fourth, there were no available measures on fetal body size, and we were therefore unable to determine whether sex differences in prenatal brain growth are independent from sex differences in overall body growth. Nonetheless, it is noteworthy that prior studies on the neonatal period have reported that sex differences in brain size persist even after accounting for sex differences in birth weight[53]. Finally, the present research reports only one of many brain growth metrics. Further research incorporating additional neuroanatomical, diffusion-weighted, and functional measures will be important for gaining a more comprehensive understanding of perinatal brain development.

A considerable strength of the present research is the comparatively large sample size, making this one of the largest known studies on perinatal brain development. Importantly, this is also one of the few studies to analyse both prenatal and postnatal brain development at the same time, allowing us to map continuous perinatal growth trajectories. Additionally, while various existing studies on postnatal development begin from a few weeks after birth, the neonatal scans used in this research begin from day 0, capturing brain growth during the early neonatal period. The dHCP structural pre-processing pipeline[54] used in this research is optimised for the studied period and overcomes several challenges typically encountered in prenatal and neonatal brain imaging (e.g., partial volume effects, low tissue contrast, motion artefacts). Importantly, both fetal and neonatal scans were pre-processed using the largely similar pipelines and segmentations, facilitating comparability across these life stages.

In summary, using one of the largest prenatal and neonatal MRI datasets, our findings highlight changes in volumetric dynamics as the brain transitions from the prenatal to the postnatal stage. The identified patterns show earliest peak growth for white matter during the second trimester, followed by subcortical gray matter during the third trimester and, lastly, cortical gray matter postnatally. Moreover, our findings indicate that shifts in volumetric dynamics predominantly occur during the final stages of gestation, suggesting that they are likely initiated by the prenatal environment in anticipation of birth. The studied age range also captured one of the critical periods for differential growth between males and females, with the timeline of the observed sex differences corresponding with the timeline of prenatal sex hormone fluctuations. Overall, the identification of these patterns emphasises the importance of integrating the prenatal and postnatal periods to facilitate a more comprehensive and continuous understanding of early growth trajectories.

	Range	Mean (SD) all	Mean (SD) males	Mean (SD) females	Sex differences *p* values
Postconceptional age at scan—all scans	21.14–44.71	37.43 (6.36)	37.45 (6.25)	37.46 (6.50)	0.92
Postconceptional age at scan—prenatal scans	21.14–38.29	29.17 (3.90)	29.24 (3.85)	29.08 (3.97)	0.72
Postconceptional age at scan—postnatal scans	37.43–44.86	41.50 (1.65)	41.38 (1.60)	41.62 (1.71)	0.08
Gestational age at birth—postnatal scans	37–43	40.11 (1.18)	40.07 (1.15)	40.14 (1.22)	0.48
Postnatal age at scan—postnatal scans	0–49	9.69 (9.44)	9.15 (8.91)	10.33 (10.00)	0.15
Birth weight—postnatal scans	1.82–5.36	3.58 (0.55)	3.65 (0.55)	3.49 (0.55)	0.002

Table 3. Sample characteristics. Sample characteristics for the full sample, also stratified by sex assigned at birth. P values for sex differences in sample characteristics, based on two-sample t-tests, are also reported. SD, standard deviation.

Methods

Participants

Participants were recruited as part of the developing Human Connectome Project (dHCP)[25]. The project was ethically approved by the UK National Research Ethics Authority (14/LO/1169), and all experiments were performed in accordance with the specified guidelines and regulations. Written informed consent was obtained from the parents or legal guardians of the infants.

In total, the dHCP dataset consists of 783 neonatal scans and 273 prenatal scans. Exclusion criteria employed for this study included multiple births, brain anomalies with likely analytical and clinical significance, any pregnancy or neonatal clinical complications, and preterm births (< 37 weeks gestational age) for neonatal scans. The final sample used in the analysis consisted of 798 scans from 699 unique fetuses/neonates (380 males and 319 females, as assigned at birth) spanning a post-conceptional age range of 21.14 to 44.71 weeks. Amongst these were 263 fetal scans from 244 fetuses (131 males and 113 females) and 535 neonatal scans from 533 neonates (287 males and 246 females). Full sample characteristics are reported in Table 3. A subset of the sample ($N = 97$) had longitudinal scans, of which 78 participants had both fetal and neonatal scans, 16 participants had 2 fetal scans, 1 participant had 3 fetal scans, and 2 participants had 2 neonatal scans.

Data acquisition and preprocessing

Prenatal scans

All imaging data were acquired using a Philips Achieva 3T MRI scanner (Philips Medical Systems) with R3.2.2 software. Mothers were placed in a supine position, and their blood pressure and peripheral pulse oximetry was monitored throughout the scan. Structural T2-weighted (T2w) images were collected using a multi-band 2, single-shot Fast Spin Echo (ssFSE) sequence, which included an MB tip-back pulse to enhance signal-to-noise ratio (SNR). Data were collected from six uniquely oriented stacks centred on the fetal brain using the following parameters: Resolution = 1.5 × 1.5 × 4.0 mm (− 1.1 gap), TR/TE = 2265+/250 ms. Localised B1 + shimming was performed to optimise magnetic field uniformity, while B0 shimming was performed to correct for field sensitivity introduced by the tip-back preparation pulse.

3D T2w images were reconstructed with a 1.0 mm resolution from motion-affected ssFSE stacks using an automated slice-to-volume registration (SVR) pipeline. The processing pipeline included denoising, inhomogeneity correction using B1 + calibration, brain localisation via V-net, and multiple iterations of SVR and super-resolution reconstruction. Afterwards, the 3D images were reoriented to standard anatomical planes using a transformer network specifically designed for the fetal brain. Cubic interpolation was then applied to achieve a final resolution of 0.5 × 0.5 × 0.5 mm.

Neonatal scans

Imaging was performed on the same scanner using the dHCP neonatal brain imaging system, which featured a neonatal 32-channel phased array head coil and a custom-designed patient handling system from Rapid Biomedical GmbH (Rimpar, Germany). Infants were fed, swaddled, and then scanned without sedation. Earplugs (President Putty, Coltene Whaledent, Mahwah, NJ, USA) and neonatal earmuffs (MiniMuffs, Natus Medical Inc., San Carlos, CA, USA) were used for auditory protection. Heart rate, oxygen saturation, and temperature were monitored throughout the scan by a paediatrician or neonatal nurse.

As described in the dHCP protocol, a Cramer Rao Lower bound approach was used to maximise contrast to noise ratio. T2w inversion recovery Fast Spin Echo (FSE) sequences were acquired in sagittal and axial orientations. Relaxation times were set to 1800/150 ms for gray matter and 2500/250 ms for white matter[55]. The in-plane resolution was set to 0.8 × 0.8 mm^2, with a slice thickness of 1.6 mm and a slice overlap of 0.8 mm. Other parameters were as follows for T2w images: TR/TE = 12,000/156 ms, SENSE factor 2.11 (axial) and 2.60 (sagittal).

The acquisitions were reconstructed using a motion correction algorithm, and transverse and sagittal images were fused into a single 3D volume for high resolution and accurate volume estimation[54].

Data preprocessing

Similar pre-processing procedures were used for both the prenatal and neonatal scans based on the dHCP structural pre-processing pipeline[54]. In summary, the T2w images were motion-corrected, bias-corrected, and brain-extracted[57]. Next, a probabilistic tissue atlas was registered to the corrected images. The Draw-EM

algorithm[58] was then used for initial tissue segmentation into CSF, white matter, cortical gray matter, and subcortical gray matter. Subsequently, labelled atlases[59] were registered to the images using both T2w images and gray matter probability maps from the initial segmentation. The final segmentation consisted of 87 Gy and white matter structures[58–60]. Additional segmentation labels were available for the fetal scans, though these were not used in this analysis for the purposes of consistency with the neonatal segmentation. All fetal segmentations were also reviewed for anatomical accuracy, and labelling errors were manually corrected by a neuroscientist with expertise in fetal neuroanatomy. Preprocessing codes are all available online (https://github.com/BioMedIA/dhcp-structural-pipeline, https://github.com/MIRTK/DrawEM/tree/feature/fetal_segmentation).

Analysis

Statistical analyses were conducted on R (version 4.3.3, 2024-02-29)[61], using the packages *nlme*, *tidyverse*, and *ggplot2*. Mixed-effects models, with random intercepts modelled at the subject-level, were used to assess the effects of age, sex, and sex-by-age interactions on brain volumes. Additionally, in order to understand relative growth, regions and tissues were analysed as a proportion of total brain volume (regional analyses presented in supplementary materials). A Benjamini–Hochberg false discovery rate (FDR) correction was applied to each analysis category using a significance threshold of 0.05[27]. FDR corrections were applied separately for absolute and proportional analyses, as well as for global and regional analyses. A total of 87 cortical and subcortical gray and white matter structures were tested.

Model comparisons

Given the nonlinear nature of brain growth, polynomial models were considered to capture more complex growth trajectories. Prior to the analyses, Bayesian Information Criterion (BIC) values were computed for each brain measure (separately for absolute and proportional volumes) to determine whether a linear, quadratic, or cubic model best described its growth trajectory (Supplementary Tables 3 and 4). Compared to Akaike Information Criterion (AIC), BIC imposes greater penalties for model complexity to minimise overfitting and is recommended in scenarios where the primary aim is to select a model that best fits existing data as opposed to one that best predicts future observations[62]. Mixed-effects models were then fit to each brain measure using the model type with the lowest BIC value. To reduce multicollinearity in the polynomial models, postconceptional age at scan was mean-centred. The models were defined as follows:

$$Linear:\ Y_i = \beta_0 + \beta_1 \cdot Age_i + \beta_2 \cdot Sex_i + \beta_3 \cdot (Age_i\ x\ Sex_i) + \mu_i + \in_i$$

$$\begin{aligned} Quadratic:\ Y_i &= \beta_0 + \beta_1 \cdot Age_i + \beta_2 \cdot Age_i^2 + \beta_3 \cdot Sex_i \\ &+\beta_4 \cdot (Age_i\ x\ Sex_i) + \beta_5 \cdot \left(Age_i^2 x\ Sex_i\right) + \mu_i + \in_i \end{aligned}$$

$$\begin{aligned} Cubic:\ Y_i &= \beta_0 + \beta_1 \cdot Age_i + \beta_2 \cdot Age_i^2 + \beta_3 \cdot Age_i^3 \\ &+\beta_4 \cdot Sex_i + \beta_5 \cdot (Age_i\ x\ Sex_i) + \beta_6 \cdot \left(Age_i^2 x\ Sex_i\right) \\ &+\beta_6 \cdot \left(Age_i^3 x\ Sex_i\right) + \mu_i + \in_i \end{aligned}$$

where:

$$Y_i = brain\ volume,\ \beta = coefficient,\ \mu_i = random\ intercept\ for\ subjects,\ \in_i = error\ terms$$

The same models were applied for proportional growth trajectories, where Y_i represents the tissue or region as a proportion of total brain volume:

$$Proportional\ Volume = \frac{Regional\ Volume}{Total\ Brain\ Volume}$$

Standardised beta coefficients were also calculated for all analyses by z-scoring the data and are reported fully in the Supplementary Materials.

Variance modelling

As is well-documented in early developmental research[8,18], the sample showed increasing variance in volumes with age. Visual inspection of the residual plots revealed a funnel-like shape, where the residual variance increased with age. To account for this, power variance weighting was applied using the *varPower* function in *nlme*. In this technique, each observation is weighted inversely proportional to a transformation of its variance, where the transformation is defined by a power function. This approach stabilises variance across ages, addressing heteroscedasticity and producing more reliable model estimates[63].

Growth metrics

Peak growth points were calculated to identify the periods of most rapid growth within the studied age range. For quadratic models, peak growth points occurred at the extreme ends of the studied age range (beginning of the range for negative quadratic terms and end of the range for positive terms). For cubic models, peak growth points were determined via calculating the postconceptional age corresponding to the highest value of the first derivative.

Sensitivity analyses

To account for postnatal age at scan for the neonatal scans, we extracted fitted values from models that regressed the brain volumes of interest on postnatal age at scan. This approach was used to maintain consistency across the analyses as postnatal age at scan is not applicable to prenatal scans and therefore could not be included as a covariate in the overall model. We also ran extended model comparisons that also included logarithmic and exponential models to ensure that the selected models were the best fit to the data.

Data availability

The data analysed in the manuscript is publicly available can be accessed via the Developing Human Connectome Project: (https://www.developingconnectome.org).

Received: 9 May 2025; Accepted: 23 December 2025
Published online: 15 January 2026

References

1. Ackerman, S. The development and shaping of the brain. In *Discovering the Brain* (National Academies Press (US), 1992).
2. Estrin, G. L. & Bhavnani, S. Brain development: structure. In *Encyclopedia of Infant and Early Childhood Development*, 2nd edn. (ed Benson, J. B.) 205–214. https://doi.org/10.1016/B978-0-12-809324-5.23776-0 (Elsevier, 2020).
3. Gilmore, J. H., Knickmeyer, R. C. & Gao, W. Imaging structural and functional brain development in early childhood. *Nat. Rev. Neurosci.* **19**, 123–137 (2018).
4. Raznahan, A., Greenstein, D., Lee, N. R., Clasen, L. S. & Giedd, J. N. Prenatal growth in humans and postnatal brain maturation into late adolescence. *Proc. Natl. Acad. Sci.* **109**, 11366–11371 (2012).
5. de Mendonça Filho, E. J. et al. Cognitive development and brain Gray matter susceptibility to prenatal adversities: moderation by the prefrontal cortex brain-Derived neurotrophic factor gene Co-expression network. *Front. Neurosci.* **15**, (2021).
6. Alex, A. M. et al. Genetic influences on the developing young brain and risk for neuropsychiatric disorders. *Biol. Psychiatry*. **93**, 905–920 (2023).
7. Holland, D. et al. Structural growth trajectories and rates of change in the first 3 months of infant brain development. *JAMA Neurol.* **71**, 1266–1274 (2014).
8. Kyriakopoulou, V. et al. Normative biometry of the fetal brain using magnetic resonance imaging. *Brain Struct. Funct.* **222**, 2295–2307 (2017).
9. Andescavage, N. N. et al. Complex trajectories of brain development in the healthy human fetus. *Cereb. Cortex.* **27**, 5274–5283 (2017).
10. Scott, J. A. et al. Growth trajectories of the human fetal brain tissues estimated from 3D reconstructed in utero MRI. *Int. J. Dev. Neurosci.* **29**, 529–536 (2011).
11. Vasung, L. et al. Quantitative in vivo MRI assessment of structural asymmetries and sexual dimorphism of transient fetal compartments in the human brain. *Cereb. Cortex*. **30**, 1752–1767 (2020).
12. Mihailov, A. et al. Normative models combining fetal and postnatal MRI data to characterize neurodevelopmental trajectories during the transition from in- to ex-utero. 2024.03.07.583908. https://doi.org/10.1101/2024.03.07.583908 (2024).
13. Casey, B. J., Tottenham, N., Liston, C. & Durston, S. Imaging the developing brain: what have we learned about cognitive development? *Trends Cogn. Sci.* **9**, 104–110 (2005).
14. Fitzgerald, E., Hor, K. & Drake, A. J. Maternal influences on fetal brain development: the role of nutrition, infection and stress, and the potential for intergenerational consequences. *Early Hum. Dev.* **150**, 105190 (2020).
15. van Dyck, L. I. & Morrow, E. M. Genetic control of postnatal human brain growth. *Curr. Opin. Neurol.* **30**, 114–124 (2017).
16. Ruigrok, A. N. V. et al. A meta-analysis of sex differences in human brain structure. *Neurosci. Biobehav. Rev.* **39**, 34–50 (2014).
17. Sex, D. in Human Brain Structure at Birth | Biology of Sex Differences | Full Text. https://bsd.biomedcentral.com/articles/https://doi.org/10.1186/s13293-024-00657-5
18. Studholme, C., Kroenke, C. D. & Dighe, M. Motion corrected MRI differentiates male and female human brain growth trajectories from mid-gestation. *Nat. Commun.* **11**, 3038 (2020).
19. Auyeung, B., Lombardo, M. V. & Baron-Cohen, S. Prenatal and postnatal hormone effects on the human brain and cognition. *Pflugers Arch.* **465**, 557–571 (2013).
20. Hines, M. Neuroscience and sex/gender: looking back and forward. *J. Neurosci. Off. J. Soc. Neurosci.* **40**, 37–43 (2020).
21. Terasaki, L. S., Gomez, J. & Schwarz, J. M. An examination of sex differences in the effects of early-life opiate and alcohol exposure. *Philos. Trans. R Soc. Lond. B Biol. Sci.* **371**, 20150123 (2016).
22. Bao, A. M. & Swaab, D. F. Sexual differentiation of the human brain: relation to gender identity, sexual orientation and neuropsychiatric disorders. *Front. Neuroendocrinol.* **32**, 214–226 (2011).
23. Loomes, R., Hull, L. & Mandy, W. P. L. What is the male-to-female ratio in autism spectrum disorder? A systematic review and meta-analysis. *J. Am. Acad. Child. Adolesc. Psychiatry*. **56**, 466–474 (2017).
24. Baron-Cohen, S. et al. Why are autism spectrum conditions more prevalent in males? *PLoS Biol.* **9**, e1001081 (2011).
25. Floris, D. L. et al. Towards robust and replicable sex differences in the intrinsic brain function of autism. *Mol. Autism*. **12**, 19 (2021).
26. Edwards, A. D. et al. The developing human connectome project neonatal data release. *Front. Neurosci.* **16**, 886772 (2022).
27. Benjamini, Y. & Hochberg, Y. Controlling the false discovery rate: a practical and powerful approach to multiple testing. *J. R Stat. Soc. B.* **57**, 289–300 (1995).
28. Nelson, M. D., Tavaré, C. J., Petrus, L., Kim, P. & Gilles, F. H. Changes in the size of the lateral ventricles in the normal-term newborn following vaginal delivery. *Pediatr. Radiol.* **33**, 831–835 (2003).
29. Huang, H. et al. White and Gray matter development in human fetal, newborn and pediatric brains. *NeuroImage* **33**, 27–38 (2006).
30. Bayer, S. A. & Altman, J. *The Human Brain During the Third Trimester* (CRC, 2003). https://doi.org/10.1201/9780203494943
31. Counsell, S. J. et al. Diffusion-weighted imaging of the brain in preterm infants with focal and diffuse white matter abnormality. *Pediatrics*. **112**, 1–7 (2003).
32. Knickmeyer, R. C. et al. A structural MRI study of human brain development from birth to 2 years. *J. Neurosci. Off J. Soc. Neurosci.* **28**, 12176–12182 (2008).
33. Bethlehem, R. A. I. et al. Brain charts for the human lifespan. *Nature*. **604**, 525–533 (2022).
34. Gilmore, J. H. et al. Regional Gray matter Growth, sexual Dimorphism, and cerebral asymmetry in the neonatal brain. *J. Neurosci.* **27**, 1255–1260 (2007).
35. Boardman, J. P. et al. Abnormal deep grey matter development following preterm birth detected using deformation-based morphometry. *NeuroImage* **32**, 70–78 (2006).
36. Loh, W. Y. et al. Neonatal basal ganglia and thalamic volumes: very preterm birth and 7-year neurodevelopmental outcomes. *Pediatr. Res.* **82**, 970–978 (2017).

37. Bolduc, M. E. et al. Regional cerebellar volumes predict functional outcome in children with cerebellar malformations. *Cerebellum Lond. Engl.* **11**, 531–542 (2012).
38. Niu, P. P., Wang, X. & Xu, Y. M. Causal effects of serum testosterone levels on brain volume: a sex-stratified Mendelian randomization study. *J. Endocrinol. Investig.* **46**, 1787–1798 (2023).
39. Perrin, J. S. et al. Growth of white matter in the adolescent brain: role of testosterone and androgen receptor. *J. Neurosci.* **28**, 9519–9524 (2008).
40. Kelava, I., Chiaradia, I., Pellegrini, L., Kalinka, A. T. & Lancaster, M. A. Androgens increase excitatory neurogenic potential in human brain organoids. *Nature* **602**, 112–116 (2022).
41. Pavlinek, A. et al. Using organoids to model sex differences in the human brain. *Biol. Psychiatry Glob. Open. Sci.* **4**, 100343 (2024).
42. Aydin, E. et al. Fetal anogenital distance using ultrasound. *Prenat Diagn.* **39**, 527–535 (2019).
43. Gennatas, E. D. et al. Age-related effects and sex differences in gray matter density, volume, mass, and cortical thickness from childhood to young adulthood. *J. Neurosci. Off. J. Soc. Neurosci.* **37**, 5065–5073 (2017).
44. Peper, J. S., Pol, H., Crone, H. E., van Honk, J. & E. A. & Sex steroids and brain structure in pubertal boys and girls: a mini-review of neuroimaging studies. *Neuroscience* **191**, 28–37 (2011).
45. Sisk, C., Lonstein, J. S. & Gore, A. C. Critical periods during development: hormonal influences on neurobehavioral transitions across the life span. In *Neuroscience in the 21st Century: from Basic to Clinical* (ed Pfaff, D. W.) 1715–1752. https://doi.org/10.1007/978-1-4614-1997-6_61 (Springer, 2013).
46. Lotze, M. et al. Novel findings from 2,838 adult brains on sex differences in Gray matter brain volume. *Sci. Rep.* **9**, 1671 (2019).
47. Stevens, F. L., Hurley, R. A. & Taber, K. H. Anterior cingulate cortex: unique role in cognition and emotion. *J. Neuropsychiatry Clin. Neurosci.* **23**, 121–125 (2011).
48. Apps, M. A. J., Rushworth, M. F. S. & Chang, S. W. C. The anterior cingulate gyrus and social cognition: tracking the motivation of others. *Neuron* **90**, 692–707 (2016).
49. Proverbio, A. M. Sex differences in social cognition. In *Social and Affective Neuroscience of Everyday Human Interaction: from Theory to Methodology* (eds Boggio, P. S. et al.) 85–106. https://doi.org/10.1007/978-3-031-08651-9_6 (Springer International Publishing, 2023).
50. Beesdo, K., Pine, D. S., Lieb, R. & Wittchen, H. U. Incidence and risk patterns of anxiety and depressive disorders and categorization of generalized anxiety disorder. *Arch. Gen. Psychiatry.* **67**, 47–57 (2010).
51. Searle, S. R., Casella, G. & McCulloch, C. Wiley, E. Variance Components. (1992).
52. Gurleyik, K. & Haacke, E. M. Quantification of errors in volume measurements of the caudate nucleus using magnetic resonance imaging. *J. Magn. Reson. Imaging.* **15**, 353–363 (2002).
53. Khan, Y. T. et al. Sex differences in human brain structure at birth. *Biol. Sex. Differ.* **15**, 1–14 (2024).
54. Makropoulos, A. et al. The developing human connectome project: A minimal processing pipeline for neonatal cortical surface reconstruction. *NeuroImage.* **173**, 88–112 (2018).
55. Williams, L. A. et al. Neonatal brain: regional variability of in vivo MR imaging relaxation rates at 3.0 T–initial experience. *Radiology.* **235**, 595–603 (2005).
56. Cordero-Grande, L. et al. Sensitivity encoding for aligned multishot magnetic resonance reconstruction. *IEEE Trans. Comput. Imaging.* **2**, 266–280 (2016).
57. Smith, S. M. Fast robust automated brain extraction. *Hum. Brain Mapp.* **17**, 143–155 (2002).
58. Makropoulos, A. et al. Automatic whole brain MRI segmentation of the developing neonatal brain. *IEEE Trans. Med. Imaging.* **33**, 1818–1831 (2014).
59. Gousias, I. S. et al. Magnetic resonance imaging of the newborn brain: automatic segmentation of brain images into 50 anatomical regions. *PLoS One.* **8**, e59990 (2013).
60. Bozek, J. et al. Construction of a neonatal cortical surface atlas using multimodal surface matching in the developing human connectome project. *NeuroImage.* **179**, 11–29 (2018).
61. Ihaka, R. & Gentleman, R. R. A language for data analysis and graphics. *J. Comput. Graph. Stat.* **5**, 299–314 (1996).
62. Chakrabarti, A., Ghosh, J. K. & AIC BIC and recent advances in model selection. In *Philosophy of Statistics*, vol. 7 (eds Bandyopadhyay, P. S. & Forster, M. R.) 583–605 (North-Holland, 2011).
63. Pinheiro, J. et al. *nlme: Linear and Nonlinear Mixed Effects Models*, R package version 3.1-167 (1999). https://doi.org/10.32614/CRAN.package.nlme

Acknowledgements

We thank Lena Dorfschmidt for providing a pre-processing script that aided the extraction of brain volume measurements for this analysis. These results were obtained using data made available from the Developing Human Connectome Project. Data used in the preparation of this manuscript were obtained from the National Institute of Mental Health (NIMH) Data Archive (NDA). NDA is a collaborative informatics system created by the National Institutes of Health to provide a national resource to support and accelerate research in mental health. Dataset identifier(s): 3995. This manuscript reflects the views of the authors and may not reflect the opinions or views of the NIH or of the Submitters submitting original data to NDA.

Author contributions

Design and conceptualisation—Y.T.K, A.T, C.A., M.A.R., R.A.I.B, M-C.L., S.B-C. Data processing: Y.T.K and A.T. Analysis: Y.T.K. Writing—original draft: Y.T.K. Writing—reviewing and editing: Y.T.K, A.T, C.A., M.A.R., R.A.I.B, M-C.L., S.B-C.

Funding

These results were obtained using data made available from the Developing Human Connectome Project funded by the European Research Council under the European Union's Seventh Framework Programme (FP/2007–2013) / ERC Grant Agreement no. [319456]. Y.T.K is supported by the Cambridge Trust and Trinity College, Cambridge. SBC received funding from the Wellcome Trust 214322\Z\18\Z. For the purpose of Open Access, the author has applied a CC BY public copyright licence to any Author Accepted Manuscript version arising from this submission. SBC also received funding from the Innovative Medicines Initiative 2 Joint Undertaking under grant agreement No 777394 for the project AIMS-2-TRIALS. This Joint Undertaking receives support from the European Union's Horizon 2020 research and innovation programme and EFPIA and AUTISM SPEAKS, Autistica, SFARI. SBC also received funding from Autism Action, SFARI, the Templeton World Charitable Fund and the MRC. The funders had no role in the design of the study; in the collection, analyses, or interpretation of data; in the writing of the manuscript, or in the decision to publish the results. Any views expressed are those

of the author(s) and not necessarily those of the funders (including IHI-JU2). All research at the Department of Psychiatry in the University of Cambridge is supported by the NIHR Cambridge Biomedical Research Centre (NIHR203312) and the NIHR Applied Research Collaboration East of England. The views expressed are those of the author(s) and not necessarily those of the NIHR or the Department of Health and Social Care. M.-C.L. is supported by a Canadian Institutes of Health Research Sex and Gender Science Chair (GSB 171373).

Declarations

Competing interests

R.A.I.B. is a director of and holds equity in Centile Bioscience Ltd. All other authors declare that they have no competing interests.

Additional information

Supplementary Information The online version contains supplementary material available at https://doi.org/10.1038/s41598-025-33981-w.

Correspondence and requests for materials should be addressed to Y.T.K.

Reprints and permissions information is available at www.nature.com/reprints.

Publisher's note Springer Nature remains neutral with regard to jurisdictional claims in published maps and institutional affiliations.